

“I May Not Have Articulated Myself Clearly”: Diagnosing Dynamic Instability in LLM Reasoning at Inference Time

Jinkun Chen¹ Fengxiang Cheng^{2,3} Sijia Han⁴ Vlado Keselj¹

Abstract

Reasoning failures in large language models (LLMs) are typically measured only at the end of a generation, yet many failures manifest as a process-level breakdown: the model “loses the thread” mid-reasoning. We study whether such breakdowns are detectable from inference-time observables available in standard APIs (token log probabilities), without any training or fine-tuning. We define a simple instability signal that combines consecutive-step distributional shift (JSD) and uncertainty (entropy), summarize each trace by its peak instability strength, and show that this signal reliably predicts failure. Across GSM8K and HotpotQA, instability strength predicts wrong answers with above-chance AUC and yields monotonic bucket-level accuracy decline at scale across model sizes. Crucially, we show that instability is not uniformly harmful: early instability can reflect subsequent stabilization and a correct final answer (*corrective instability*), whereas late instability is more often followed by failure (*destructive instability*), even at comparable peak magnitudes, indicating that recoverability depends not only on how strongly the distribution changes but also on when such changes occur relative to the remaining decoding horizon. The method is model-agnostic, training-free, and reproducible, and is presented as a diagnostic lens rather than a corrective or control mechanism.

1. Introduction

LLM reasoning failures are typically evaluated as end-point errors, yet the generation process is a temporal dynamical system whose internal evolution can become unstable. We study whether inference-time signals can distinguish a class

¹Dalhousie University ²University of Amsterdam ³Tsinghua University ⁴Meta. Correspondence to: Jinkun Chen <jinkun.chen@dal.ca>.

Preprint. February 4, 2026.

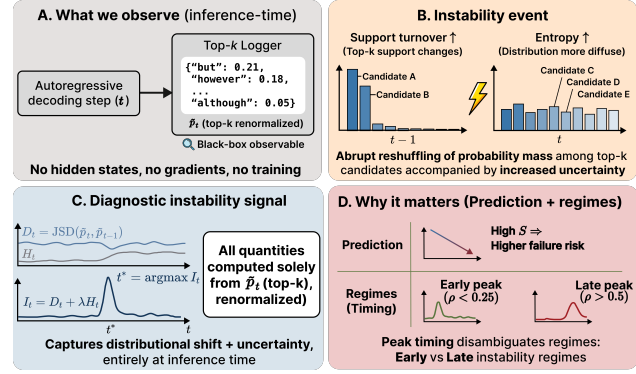


Figure 1. Inference-time dynamic instability as a diagnostic signal. Conceptual overview of an inference-time diagnostic for dynamic instability in large language model reasoning. **A:** At each decoding step t , we observe only the renormalized top- k next-token distribution \tilde{p}_t , which is accessible as a black-box inference-time signal; no hidden states, gradients, or training access are required. **B:** An instability event is characterized by an abrupt reshuffling of probability mass among high-probability candidates, accompanied by increased uncertainty (higher entropy) between consecutive steps. **C:** We define a diagnostic instability signal $I_t = D_t + \lambda H_t$, combining distributional shift $D_t = \text{JSD}(\tilde{p}_t, \tilde{p}_{t-1})$ and uncertainty H_t . All quantities are computed solely from \tilde{p}_t at inference time, with overall instability strength summarized as $S = \max_t I_t$. **D:** Instability strength S is associated with increased failure risk, while the peak location (relative position ρ) provides complementary information, separating earlier (more recoverable/corrective) from later (less recoverable/destructive) instability episodes.

of failures driven by dynamic instability, rather than by static knowledge limitations. Our goal is diagnostic rather than corrective: identify process-level indicators that reliably predict failure, without modifying the model.

Motivation. In many applications, the relevant question is not only *whether* an answer is correct, but *when* the generation begins to break down and whether it is likely to recover. Final-answer accuracy is retrospective, and static confidence proxies can miss intra-trajectory transitions; conversely, multi-sample consistency methods require multiple runs. We therefore ask a minimal inference-time question: can a *single* decoding trace reveal an observable signature of unstable reasoning using only token probabilities? Figure 1 provides a conceptual overview of our inference-time diag-

nostic, illustrating what is observable at decoding time, how instability manifests in token distributions, and why instability strength and timing are predictive of reasoning failure. Unlike accuracy-oriented interventions, our analysis does not aim to improve correctness, but to characterize when and how reasoning processes become unstable. We focus on detecting and characterizing instability, not on correcting or controlling it.

To avoid confusion with related notions, our instability signal is not a confidence score, a calibration method, a hallucination detector, or a verifier. It targets trajectory-level dynamical behavior rather than outcome-level uncertainty: two traces with similar average entropy can exhibit very different instability profiles, and only the latter reflects temporal disruption during reasoning.

Why can the next-token distribution represent reasoning stability? Autoregressive decoding induces a closed-loop state evolution in which the internal state updates based on previously generated tokens, yet the model’s token distribution is the only black-box observable of this evolving state. Small perturbations may therefore be amplified over time through this feedback loop. Formally, letting h_t denote the internal state and x_t the emitted token,

$$h_{t+1} = f(h_t, x_t), \quad p_t = g(h_t), \quad (1)$$

where p_t is the full next-token distribution; in black-box settings we observe \tilde{p}_t , its top- k truncation and renormalization. We therefore study *intra-trajectory temporal instability*: abrupt changes in p_t (or \tilde{p}_t when truncated) over time *within a single trace*. This differs from self-consistency and other sampling-based methods, which analyze *inter-trajectory* variability across multiple samples. It also differs from static uncertainty: we do not treat entropy as a standalone confidence score, but combine entropy with consecutive-step distributional shifts to quantify localized regime shifts during a single generation.

Prior work shows that LLMs often fail to identify their own reasoning errors without explicit localization, motivating process-level diagnostics of reasoning traces (Tyen et al., 2023). Recent methods propose temporal signals for reasoning process error identification and visualization of reasoning paths, while uncertainty analyses highlight the limits of explanation faithfulness (Guo et al., 2025; Li et al., 2025b; Da et al., 2025). We complement these directions with an inference-time instability signal defined directly on token distributions. Figure 2 previews our central observation: instability strength alone is insufficient; its timing determines whether reasoning recovers or collapses.

Our contributions are:

1. **Inference-time instability signal.** We define a training-free instability signal $I_t = D_t + \lambda H_t$ that

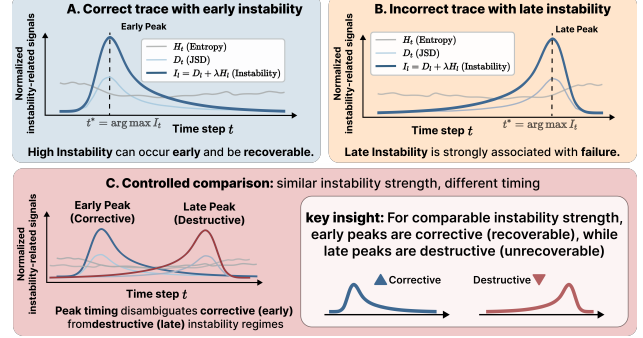


Figure 2. Timing-dependent regimes of inference-time instability. Representative decoding traces illustrating how the *timing* of instability, rather than its magnitude alone, is associated with different reasoning outcomes. **A:** A representative trace with an early instability peak (**recoverable / corrective**). Although the instability signal I_t reaches a high value, it occurs sufficiently early in decoding for the model to recover, resulting in a correct final answer. **B:** A representative trace with a late instability peak (**unrecoverable / destructive**). Despite comparable instability strength, the peak occurs near the end of decoding, leaving limited opportunity for recovery and resulting in an incorrect final answer. **C:** A controlled comparison with instability signals normalized to comparable peak strength, demonstrating that magnitude alone is insufficient: similar instability strength can correspond to different outcomes depending on peak timing. All curves show representative (not averaged) decoding trajectories, with instability defined as $I_t = D_t + \lambda H_t$.

combines consecutive-step distributional shift and uncertainty, computed solely from token log probabilities.

2. **Single-trace failure predictability.** Instability strength predicts reasoning failure from a *single* decoding trace, achieving AUC 0.66–0.74 on GSM8K and remaining predictive at scale on the full GSM8K test set and the HotpotQA distractor validation split.
3. **Timing-dependent diagnostic refinement.** We distinguish *destructive* from *corrective* instability via peak timing, showing that instability magnitude alone is insufficient and that recoverability depends on when instability occurs.

Scope. We test a single claim: instability strength increases with failure rate under both deterministic and stochastic decoding. We prioritize cross-family reproducibility (Llama/Qwen) across matched size scales (0.5B–8B) for diagnosis rather than exhaustive benchmarking.

2. Related Work

Prior work related to our diagnostic can be broadly grouped into four threads: (i) monitoring and error localization of reasoning trajectories, (ii) prompting, sampling, and lightweight adaptation for improving reasoning, (iii) uncertainty and confidence estimation for LLM outputs, and

(iv) adversarial and disruptive perturbations that probe sensitivity of decoding dynamics. In contrast, we study *intra-trajectory* temporal instability from black-box next-token distributions, without retraining, additional models, or multi-sample aggregation.

Process monitoring and error localization. Reasoning error detection and monitoring have been explored through explicit error localization and temporal consistency signals (Tyen et al., 2023; Guo et al., 2025). Visualization and structural analysis of reasoning paths provide complementary tools for interpreting failures and diagnosing process breakdowns (Li et al., 2025b; Da et al., 2025). Process supervision and verifier-style training emphasize stepwise correctness but require additional supervision or fine-tuning (Lightman et al., 2023); recent work on process reward models (PRMs) explores data-efficient stepwise verification via chain-of-thought verifiers (Khalifa et al., 2025) and studies best practices for PRM development (Zhang et al., 2025). Relatedly, Mao et al. (2026) propose viewing confidence as a temporal signal and use Signal Temporal Logic (STL) to mine temporal patterns that distinguish correct from incorrect LLM reasoning traces. While their method requires multi-sample generation and STL mining, our approach operates on a single trace and defines instability directly from consecutive-step distributional changes. Our approach is fully inference-time and training-free, and uses only token-distribution observables available during decoding.

Prompting, sampling, and lightweight adaptation. Chain-of-thought prompting can elicit multi-step reasoning (Wei et al., 2022), and sampling-based aggregation such as self-consistency improves accuracy by marginalizing over multiple traces (Wang et al., 2022). ReAct-style prompting interleaves reasoning and acting, but can be brittle in sequential settings when intermediate steps drift (Yao et al., 2022). Beyond prompting, parameter-efficient adaptation methods such as prefix-tuning (Li & Liang, 2021), prompt tuning (Lester et al., 2021), and LoRA (Hu et al., 2021) modulate model behavior with minimal parameter updates; these methods highlight that small changes in prompt/context can induce large changes in token-level dynamics. Our instability signal is complementary: rather than changing the model, we quantify distributional drift and uncertainty along the decoding trajectory. Related work also studies prompt sensitivity directly by measuring and manipulating prompt influence on model outputs (Feng et al., 2024), which supports the broader view that token-level dynamics can be highly responsive to small input perturbations. In short, self-consistency and related approaches are, by design, *inter-trajectory* techniques, whereas we diagnose *intra-trajectory* temporal stability for a single run.

Uncertainty and confidence. Black-box self-checking approaches target hallucination detection via consistency signals (Manakul et al., 2023). Confidence calibration remains an active area, with multicalibration methods proposed to improve reliability of confidence scores (Detommaso et al., 2024). Prior work also studies the extent to which model probabilities reflect epistemic uncertainty and correlate with correctness (Kadavath et al., 2022). From an information-theoretic perspective, the next-token entropy corresponds to the conditional entropy of the next symbol given the prefix in an autoregressive process (Shannon, 1948; Cover & Thomas, 2006). Sequential inference can be viewed as repeated belief updates that ideally stabilize as evidence accumulates (MacKay, 2003). Prior work leverages predictive uncertainty (e.g., entropy) as a mostly static correctness proxy (Guo et al., 2017; Malinin & Gales, 2018); we extend this view by analyzing the *temporal evolution* of uncertainty and distributional change along a single reasoning trajectory, without claiming that information theory alone proves causal failure.

Semantic-level uncertainty measures such as *semantic entropy* (uncertainty computed at the level of meaning rather than token sequences) have been proposed as principled hallucination detectors (Farquhar et al., 2024). Extensions include semantic entropy probes (SEPs) that extract semantic uncertainty from hidden states (Kossen et al., 2024), kernel-based fine-grained uncertainty quantification (Nikitin et al., 2024), efficient Bayesian estimation methods (Ciosek et al., 2025), and *semantic energy* operating on logits to capture uncertainty in scenarios where semantic entropy fails (Ma et al., 2025). Token-level hallucination detection via variance and probability signals has also been explored (Quevedo et al., 2024; Kumar, 2025; Niu et al., 2025). Recent evaluations and frameworks compare uncertainty estimation methods and emphasize remaining challenges (Bakman et al., 2024; Heo et al., 2024; Li et al., 2025a).

These methods predominantly target *static* uncertainty at the output or semantic level, often requiring multiple samples or hidden-state access. In contrast, our focus is specifically on *temporal* instability within a single decoding trace: we track how the next-token distribution changes over time, which captures a distinct failure mode (dynamic regime shifts during reasoning) that static uncertainty measures may miss.

Finally, work on self-correction reaches mixed conclusions: some studies argue that self-correction is not an inherent capability and depends on scaffolding (Huang et al., 2023; Liu et al., 2024b), while others find evidence of intrinsic self-correction under certain settings (Liu et al., 2024a). Recent work trains models to self-correct via reinforcement learning (Kumar et al., 2024), and studies of internal representations show that LLM hidden states encode information

predictive of chain-of-thought success (Afzal et al., 2025). Our “corrective vs. destructive” distinction is compatible with this picture: high-instability episodes may correspond either to beneficial revision or to divergence toward failure. Our method differs in focus: we do not attempt to produce a calibrated confidence score; instead we characterize *dynamical* instability via temporal changes in token distributions.

Adversarial and disruptive perturbations. Recent work shows that stepwise interventions can deliberately disrupt intermediate reasoning and induce downstream errors (Peng et al., 2024). This supports our framing that process-level dynamics, not only final answers, constitute a meaningful object of study, and motivates robust, inference-time diagnostics of instability. Unlike intervention work (editing/steering), this paper is diagnosis-only: we define and validate an instability signal without applying stabilization operators.

3. Method

3.1. Inference-Time Observables

As illustrated in figure 1 (A, B, and C), our instability signal is computed entirely from logged top- k next-token distributions at inference time, without access to hidden states or full logits. At each generation step t , the model produces a predictive distribution p_t over tokens. In our implementation, we only observe top- k log probabilities. Let \mathcal{V}_t be the top- k token set at step t and define the truncated, renormalized distribution \tilde{p}_t supported on \mathcal{V}_t by setting $\tilde{p}_t(x) = 0$ for $x \notin \mathcal{V}_t$ and renormalizing over \mathcal{V}_t . When computing divergences between consecutive steps, we treat \tilde{p}_t and \tilde{p}_{t-1} as distributions over the union support $\mathcal{V}_t \cup \mathcal{V}_{t-1}$ by zero-padding outside each step’s logged set (equivalently, we compute JSD over the union key set). Unless otherwise noted, we compute all observables from \tilde{p}_t ; when full vocabulary logits are available, we compute the same quantities from p_t without truncation. Our primary objective is a black-box diagnostic based only on log probabilities; therefore we treat \tilde{p}_t as the operative observable and use quantities computed from full vocabulary logits only as a validation control when available.

We compute (using natural logarithms):

$$H_t = - \sum_x \tilde{p}_t(x) \log \tilde{p}_t(x), \quad (2)$$

$$D_t = \text{JSD}(\tilde{p}_t, \tilde{p}_{t-1}), \quad (3)$$

where $\text{JSD}(P, Q) = \frac{1}{2}\text{KL}(P\|M) + \frac{1}{2}\text{KL}(Q\|M)$ and $M = \frac{1}{2}(P+Q)$. With natural logarithms, $\text{JSD}(P, Q) \in [0, \log 2]$. In all experiments we compute logarithms only on positive probabilities. We compute KL terms only where the numerator probability is positive (as in the standard definition

of KL), noting that in JSD the mixture $M = \frac{1}{2}(P+Q)$ is strictly positive wherever P or Q is positive. For numerical stability, we optionally add a small ϵ (e.g., 10^{-12}) inside logarithms; we verified this does not change results.

3.2. Instability Signal and Strength

We define instability per-step:

$$I_t = D_t + \lambda H_t, \quad (4)$$

and note that both correct and incorrect traces can exhibit high instability (figure 2, A, B, and C), motivating a focus on temporal structure beyond magnitude. We set $\lambda = 1$ as a fixed default (equal-weighting in nats) across all tasks, models, and decoding settings, and do not tune λ to avoid optimistic bias from post-hoc hyperparameter selection. We report sensitivity via a minimal ablation comparing $\lambda = 0$ (JSD only) and $\lambda = 1$ (figure 8), and additional baselines in Appendix G. For each trace, the instability strength is $S = \max_t I_t$ to capture brief spikes. To control for trace-length confounding (longer traces have more opportunities for spikes), we also report early-window maxima $S_w = \max_{t \leq w} I_t$ for pre-specified windows $w \in \{10, 20, 50, 100\}$, highlighting S_{50} as a fixed-window control (section F).

Implementation and complexity. Given per-step top- k log probabilities, we compute D_t by evaluating JSD on the union support $\mathcal{V}_t \cup \mathcal{V}_{t-1}$ via zero-padding outside each step’s logged set, and compute H_t on the renormalized \tilde{p}_t . This yields an $O(Tk)$ per-trace computation (streamable with $O(k)$ working memory), making the diagnostic practical at scale. For determinism, when taking arg max over time we break ties by the smallest t (as specified for t^* and t_{50}^*).

3.3. Theoretical Intuition

Autoregressive decoding is a closed-loop dynamical system: as the model generates tokens, it updates an unobserved internal state that determines the next-token distribution. Abrupt step-to-step shifts in the distribution are therefore natural observable signatures of internal regime changes. Our instability signal combines realized distributional change (D_t via consecutive-step JSD) with uncertainty (H_t via entropy) to capture both *route switching* and *decision fragility*. For space, we defer the full theoretical statements (including the recoverability/timing formalization) to Appendix B.

Recoverability under a finite decoding horizon (intuition). We view decoding as a finite-horizon process in which entering a stable continuation regime requires a minimum amount of time. When instability occurs early, there

remains sufficient decoding budget for the model to re-stabilize and converge to a coherent trajectory. In contrast, when instability peaks late, the remaining budget becomes insufficient for recovery, even if the magnitude of the instability is comparable.

This perspective highlights that recoverability depends not only on how strongly the model’s distribution changes, but also on when such changes occur relative to the remaining decoding horizon; we emphasize that this argument is explanatory rather than a formal proof (Appendix B).

4. Experiments

4.1. Task and Models

Datasets: GSM8K (test split) (Cobbe et al., 2021) and HotpotQA (distractor validation split) (Yang et al., 2018). For controlled GSM8K-300 experiments we use the first 300 GSM8K test examples (starting from index 0 for determinism) with Qwen2.5-1.5B-Instruct (Yang et al., 2024) and Llama-3.2-1B-Instruct (Grattafiori et al., 2024). We additionally report dense per-step baseline runs on the full GSM8K test set (1319 examples) and HotpotQA distractor validation split (7405 examples), including Llama-3.2-3B-Instruct and Llama-3.1-8B-Instruct (Grattafiori et al., 2024) (section L). Models are instruction-tuned to reduce formatting confounds; sizes span $\sim 0.5\text{B}$ – 8B to test scale robustness under a fixed diagnostic.

4.2. Prompting and Decoding

For GSM8K, prompting and scoring follow the standard format: we prompt with the question text, and a prediction is scored correct if the final extracted numeric answer matches the reference answer. We extract the last number in the model output as the predicted answer. For HotpotQA, we prompt with the question and concatenated context passages and ask for a short, direct answer; we score correctness by comparing the first line of the model output to the reference using normalized matching with a containment check. We deliberately use minimal, zero-shot prompting (no few-shot exemplars) to keep decoding dynamics comparable and avoid confounds from prompt engineering. As a result, absolute accuracy can be low for these small models; our focus is on ranking and separability (AUC, monotonic bucket trends), which is less sensitive to the overall error rate than raw accuracy and is therefore suitable for diagnostic separability.

We report greedy decoding and stochastic decoding. For GSM8K-300, we evaluate Qwen2.5-1.5B-Instruct with greedy decoding and evaluate Llama-3.2-1B-Instruct under a small decoding grid with top- p 0.9 and a fixed random seed. For Llama-3.2-1B-Instruct, we additionally evaluate $\tau = 0.3$ (top- p 0.9), yielding a small decoding grid

$\tau \in \{0.0, 0.3, 0.7\}$. In analyses that pool multiple Llama-3.2-1B-Instruct decoding settings (e.g., peak-step characteristics), we aggregate across this grid, yielding 3×300 traces in total.

4.3. Logging and Trace Length Controls

In our main experiments, we log top- k token log probabilities per-step and cap generation to 128 new tokens to reduce length confounding. In addition to top- k traces, we validate key timing findings with a held-out run that logs entropy/JSD from full vocabulary logits (no truncation; section 6). We also compute early-window versions of our strength statistic to control for trace length (see Metrics and section F). Unless otherwise noted, we log top- k distributions with $k = 50$ and report top- k sensitivity in Appendix E. For timing analyses, we additionally use fixed-window peak position (e.g., ρ_{50}) to decouple peak-timing effects from the total trace length (section M).

4.4. Metrics

We evaluate instability as a diagnostic signal rather than an intervention. Let $y \in \{0, 1\}$ be the error label ($y = 1$ if the final answer is wrong). We report:

- **Bucketed accuracy:** partition examples into five equal-sized quantile buckets by instability strength S and report accuracy per bucket.
- **Rank association:** Spearman correlation between S and correctness (encoded as 1 for correct and 0 for wrong).
- **Separability:** ROC–AUC for predicting y from S (denoted $\text{AUC}_{\text{wrong}}$).

We additionally compute early-window versions by replacing S with S_w to verify that the signal is not purely driven by longer generations (a key confound for any max-over-time statistic).

4.5. Ablations and Controls

We include a minimal ablation on the instability signal by comparing $\lambda = 0$ (JSD only) and $\lambda = 1$ (JSD+entropy). We also report a small decoding grid (temperature $\tau \in \{0.0, 0.3, 0.7\}$ with top- p 0.9) to verify robustness under stochasticity.

5. Results

5.1. Instability Strength Correlates Monotonically with Failure Rate

Instability strength shows a clear monotonic relationship with failure rate. Across models and decoding settings,

bucketed accuracy decreases as instability strength increases (figure 3). The monotonic decrease is observed under equal-sized buckets, rather than an artifact of sample imbalance. This is consistent with the primary claim that dynamically unstable trajectories are disproportionately associated with wrong final answers.

5.2. Instability Strength Separates Correct and Incorrect Reasoning

Instability strength separates correct from incorrect outputs: Spearman correlations are consistently negative and AUC_{wrong} values are consistently above chance (table 1). Early-window signals preserve predictive power, indicating the effect is not simply driven by longer generations. Bootstrap confidence intervals over examples support the stability of these trends (section H).

We reuse the same traces and vary only the analysis window to control for length. Even when restricted to the first 50 steps, instability remains predictive (e.g., $AUC \approx 0.66$ on Llama-3.2-1B-Instruct), indicating that the signal is not an artifact of longer sequences. We report explicit early-window AUC values (using S_{50}) in section F. This fixed-window evaluation directly targets the trace-length confound: longer generations provide more opportunities for a large $\max_t I_t$ even under identical per-step dynamics. For example, using S_{50} yields AUC_{wrong} of 0.605 on Qwen2.5-1.5B-Instruct greedy and 0.665 on Llama-3.2-1B-Instruct ($\tau = 0.0$) (table 6). This suggests a secondary claim: instability is detectable early, before full reasoning completion, which is valuable for diagnosis and triage. We include a full early-warning curve (varying the prefix window length) in Appendix F.

Table 1 summarizes cross-model and decoding robustness, reporting overall accuracy alongside the separability of instability strength.

Across models and decoding settings (table 1), AUC values remain stable. On Llama-3.2-1B-Instruct, the monotonic trend appears with AUC values around 0.66 (greedy) to 0.74 (stochastic). The small decoding grid ($\tau \in \{0.0, 0.3, 0.7\}$) preserves the trend: increased stochasticity reduces accuracy but does not remove the instability-failure relationship.

We additionally validate on full GSM8K and HotpotQA runs, and include a ReClor (Yu et al., 2020) check as a representative setting where the signal can weaken. ReClor is a multiple-choice logical reasoning benchmark; under our short-answer decoding and first-line matching setup, correct predictions are extremely sparse. As a result, errors are dominated by stable-but-wrong trajectories, which can induce weak or even reversed correlations between instability and correctness in this setting. Detailed tables and figures are reported in Appendix L.

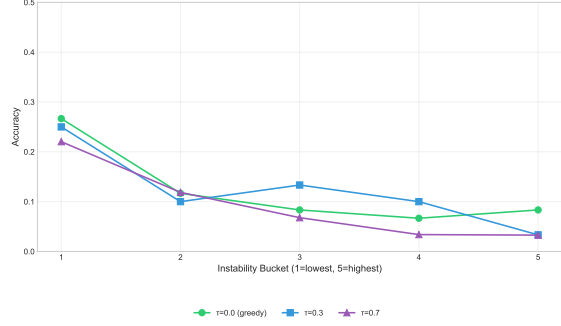


Figure 3. Monotonic bucket trends for Llama-3.2-1B-Instruct across temperature settings ($\tau \in \{0.0, 0.3, 0.7\}$). Higher instability buckets consistently show lower accuracy, confirming the predictive value of the instability signal.

5.3. Not All Instability Is Harmful

Instability magnitude alone is insufficient: some high-instability episodes reflect beneficial self-correction rather than failure. We refine diagnosis by distinguishing *corrective* versus *destructive* instability via the timing of the peak (Section 6).

5.4. Signal Ablation

Using JSD alone ($\lambda = 0$) collapses the strength distribution and yields near-random predictive power ($AUC \approx 0.52$) on Llama-3.2-1B-Instruct, while the combined signal ($\lambda = 1$) restores clear separation and monotonicity. This supports the need to combine distributional change with uncertainty.

We observe that a JSD-only signal ($\lambda = 0$) becomes nearly constant on Llama-3.2-1B-Instruct, yielding near-random separability. A plausible explanation is saturation under top- k approximations: when successive steps have weak support overlap, renormalized top- k distributions can reduce the dynamic range of divergence estimates, reducing sensitivity to more graded changes in instability. Adding entropy restores a robust signal by capturing uncertainty and competition among alternatives even when support overlap is limited. This ablation indicates that uncertainty is a necessary component of our instability proxy. We also explored change-point detectors, but found continuous strength more stable as a diagnostic signal; see section D. We additionally report time-structure negative controls and entropy-family baselines on the same traces; see section G. We include additional baseline tables and ablation figures in Appendix G.

6. Corrective vs. Destructive Instability

A critical observation emerges from our analysis: not all high-instability episodes are harmful. We identify two qualitatively distinct regimes of dynamic instability with opposite implications for reasoning outcomes. These regimes are de-

Table 1. Cross-model and decoding robustness on GSM8K (first 300 test examples; top- p 0.9 for stochastic decoding). AUC values remain stable across models and decoding settings, supporting a model-agnostic signal.

Model	Decoding	Accuracy	AUC _{wrong}	Spearman
Qwen2.5-1.5B-Inst	greedy	0.430	0.681	-0.311
Llama-3.2-1B-Inst	$\tau = 0.0$	0.123	0.657	-0.178
Llama-3.2-1B-Inst	$\tau = 0.3$	0.123	0.667	-0.190
Llama-3.2-1B-Inst	$\tau = 0.7$	0.094	0.741	-0.244

fined jointly by instability events and recoverability, rather than by instability magnitude alone.

6.1. Two Regimes of Instability

Destructive instability. Destructive instability refers to high-instability episodes that are followed by continued instability and incorrect final answers. In these traces, uncertainty tends to rise and the trajectory does not stabilize onto a coherent solution path.

Corrective instability. Corrective instability refers to high-instability episodes that are followed by stabilization and correct final answers. In these traces, uncertainty often decreases after the peak and the trajectory converges.

6.2. Operationalization

We operationalize recoverability using the **peak instability position**, which captures when the strongest instability occurs within a reasoning trace.

Given a trace $\{\tilde{p}_t\}_{t=1}^T$, let $t^* = \arg \max_t I_t$ (breaking ties by the smallest t) denote the step of peak instability. We define the relative peak position as $\rho = t^*/T$, where T is the trace length, and classify traces as:

- **Early peak** ($\rho < 0.25$): Instability occurs early, leaving time for subsequent recovery; this regime is characteristic of corrective instability.
- **Late peak** ($\rho > 0.5$): Instability occurs late, with insufficient time for recovery; this regime is characteristic of destructive instability.

We adopt coarse thresholds for interpretability (clear “early” vs. “late” separation); the qualitative ordering is robust to alternative threshold pairs and to a binned analysis of ρ (section I), and also holds under a fixed-window peak definition (section M).

This operationalization captures a simple intuition: when difficulty arises early, the model may still recover through subsequent stable reasoning, whereas late instability leaves limited opportunity for correction. Importantly, ρ is descriptive rather than causal; we do not claim that peak position

Table 2. Accuracy by peak instability position on the held-out baseline run (Llama-3.2-1B-Instruct, GSM8K, 100 traces). Early-peak traces achieve more than $3 \times$ the accuracy of late-peak traces, despite both exhibiting high instability at some point.

Peak position	% of traces	Accuracy
Early ($\rho < 0.25$)	57%	0.46
Middle ($0.25 \leq \rho \leq 0.5$)	29%	0.35
Late ($\rho > 0.5$)	14%	0.14

causes success or failure. As a control against the trivial “late means no time left” critique, we additionally measure peak position within a fixed early window and observe the same qualitative ordering (section M).

6.3. Empirical Evidence

We partition traces by peak instability position and compare their final-answer accuracy on a held-out baseline run of Llama-3.2-1B-Instruct (100 traces, logged without top- k truncation for this validation).

Table 2 shows a clear monotonic relationship between peak position and accuracy. Traces where instability peaks early have substantially higher accuracy (46%) than those where it peaks late (14%), suggesting that instability magnitude alone is an incomplete diagnostic: the *timing* and *recoverability* of instability matter. To characterize peak steps beyond timing, we also report two “low-cost probes” (margin drops and support-set turnover) in Appendix K. At the peak step, corrective traces tend to exhibit sharper probability margin drops, while destructive traces exhibit higher support-set turnover, consistent with decisive revision versus chaotic route switching (Appendix K).

We provide a visualization in Appendix A (Figure 4).

6.4. Implications

This distinction has two important implications for how inference-time instability should be interpreted. First, raw instability strength ($S = \max_t I_t$) remains a useful aggregate predictor of failure, but peak position provides a complementary summary that separates traces which recover from those that do not. This highlights that temporal

structure carries information beyond magnitude alone.

Second, our analysis clarifies the scope of this work. We do not propose or evaluate interventions; instead, our goal is diagnosis and mechanistic characterization based solely on black-box inference-time observables.

Taken together, these findings refine our central claim: while dynamic instability is predictive of failure, the underlying mechanism is nuanced. Destructive instability drives most of the predictive signal, whereas corrective instability acts as a confound that, once accounted for, sharpens the diagnostic.

7. Discussion

Takeaways. **What we showed:** inference-time instability can be detected from black-box signals (top- k token distributions) and reliably predicts reasoning failure, with consistent monotonic bucket trends and above-chance AUC across models, decoding settings, and tasks (including full-set validation on Llama-3.2-3B-Instruct and Llama-3.1-8B-Instruct). **What we clarified:** not all instability is harmful; its diagnostic meaning depends on timing, with early peaks more often followed by recovery and late peaks more often followed by failure. **What we did not claim:** we do not claim a unique internal mechanism, causality, or controllability; this paper is diagnosis-only and does not propose stabilization operators. Taken together, our results suggest that inference-time instability provides a reliable diagnostic signal for reasoning behavior, while its consequences depend critically on when it arises.

7.1. Failure Taxonomy

Our framing separates at least three conceptual failure modes. (1) *Stable-but-wrong* failures produce incorrect answers despite low instability strength S , often consistent with knowledge gaps or spurious heuristics. (2) *Dynamically unstable* failures exhibit high instability strength and cascading divergence, which is the focus of this paper. (3) *Early-collapse* failures exhibit high early-window instability (e.g., large $S_{20} = \max_{t \leq 20} I_t$) and are often tied to formatting errors or decoding pathologies. This differs from early-peak-but-recoverable cases in [section 6](#), where early instability is followed by stabilization and correct completion. This taxonomy clarifies that instability is a specific diagnostic dimension, not a universal explanation of failure.

We provide a breakdown figure in [Appendix A](#) ([Figure 5](#)).

7.2. Mechanistic Interpretation

The instability signal is purely inference-time and black-box: it uses only per-step token probabilities. Mechanistically, spikes can reflect *route switching* (abrupt changes in which continuation is locally preferred) and *decision fragility* (near

ties among candidates). We provide a longer interpretation, together with the supporting “low-cost probes”, in [Appendix J](#).

8. Limitations

First, not all failures are dynamic; stable-but-wrong cases exist and are not addressed by instability signals. Second, change-point detection is sensitive to detector choice and thresholding, making binary change-point labels less reliable than continuous strength. Third, our approach assumes that relative changes in model probabilities carry meaningful information about underlying state transitions. While we do not require perfect probability calibration, future work can study how calibration quality affects this diagnostic signal. Finally, this study focuses on a single primary task (GSM8K) for controlled grid experiments on two small models, with additional full-set runs on GSM8K and HotpotQA that include Llama-3.2-3B-Instruct and Llama-3.1-8B-Instruct. Broader evaluation across tasks and larger models is left to future work but is not necessary to validate the central mechanism. These limitations are inherent to a diagnostic perspective and do not detract from the goal of identifying dynamically unstable reasoning failures.

When the signal weakens. The signal targets dynamically unstable failure modes and can be weaker when *stable-but-wrong* errors dominate. Concretely, on ReClor in our setting, higher instability tends to correlate with correctness ($AUC_{\text{wrong}} < 0.5$). The signal also weakens when the logged top- k list is too small to estimate entropy/JSD reliably ([Appendix E](#)).

9. Conclusion

We provide a simple and reproducible inference-time diagnostic for dynamic instability in LLM reasoning. Instability strength yields a robust, monotonic relationship with failure rate and predicts errors with AUC in the range 0.57 to 0.78 across GSM8K and HotpotQA, using controlled GSM8K-300 runs and dense baseline runs at full-set scale.

Crucially, we show that not all instability is harmful: *corrective* instability reflects beneficial self-correction and is associated with higher accuracy, while *destructive* instability drives the failure-predictive signal. Peak-step probes further indicate that corrective traces exhibit sharper margin drops, while destructive traces exhibit higher support-set turnover. We report these “low-cost probes” and a longer mechanistic interpretation in [Appendix J](#) and [Appendix K](#). Taken together, these results establish instability strength and peak position as robust, black-box diagnostics of reasoning breakdowns.

Impact Statement

This work aims to advance the understanding of inference-time behavior in large language models by introducing a diagnostic signal for identifying dynamic instability during reasoning. The proposed method is purely observational, operates entirely at inference time, requires no model modification or retraining, and is intended as an analysis tool rather than a corrective or control mechanism.

Potential positive impacts include improved transparency and diagnostic assessment of LLM reasoning processes, which may support evaluation, debugging, and risk-aware deployment, particularly in settings where reasoning failures are costly. By distinguishing between corrective and destructive instability, the work also cautions against interpreting all forms of instability as uniformly harmful.

We emphasize that the method is not designed for influencing model behavior, automating decisions, or surveilling users, and it does not provide mechanisms for steering or modifying model outputs. Accordingly, we do not identify new ethical risks beyond those already associated with large language models. Any downstream use of inference-time diagnostics should be considered within appropriate task-specific and human-in-the-loop evaluation frameworks.

References

Afzal, A., Matthes, F., Chechik, G., and Ziser, Y. Knowing before saying: LLM representations encode information about chain-of-thought success before completion. In *Findings of the Association for Computational Linguistics: ACL 2025*, pp. 12791–12806, 2025. doi: 10.18653/v1/2025.findings-acl.662. URL <https://aclanthology.org/2025.findings-acl.662/>.

Bakman, Y. F., Yaldiz, D. N., Buyukates, B., Tao, C., Dimitriadis, D., and Avestimehr, S. MARS: Meaning-aware response scoring for uncertainty estimation in generative LLMs. In *Proceedings of the 62nd Annual Meeting of the Association for Computational Linguistics (Volume 1: Long Papers)*, pp. 7752–7767, 2024. doi: 10.18653/v1/2024.acl-long.419. URL <https://aclanthology.org/2024.acl-long.419/>.

Ciosek, K., Felicioni, N., and Ghiassian, S. Hallucination detection on a budget: Efficient Bayesian estimation of semantic entropy. *arXiv preprint arXiv:2504.03579*, 2025.

Cobbe, K., Kosaraju, V., Bavarian, M., Chen, M., Jun, H., Kaiser, L., Plappert, M., Tworek, J., Hilton, J., Nakano, R., Hesse, C., and Schulman, J. Training verifiers to solve math word problems. *arXiv preprint arXiv:2110.14168v2*, 2021.

Cover, T. M. and Thomas, J. A. *Elements of Information Theory*. Wiley-Interscience, 2 edition, 2006. ISBN 9780471241959.

Da, L., Liu, X., Dai, J., Cheng, L., Wang, Y., and Wei, H. Understanding the uncertainty of LLM explanations: A perspective based on reasoning topology. *arXiv preprint arXiv:2502.17026v2*, 2025.

Detommaso, G., Bertran, M., Fogliato, R., and Roth, A. Multicalibration for confidence scoring in LLMs. *arXiv preprint arXiv:2404.04689v1*, 2024.

Farquhar, S., Kossen, J., Kuhn, L., and Gal, Y. Detecting hallucinations in large language models using semantic entropy. *Nature*, 630:625–630, 2024. doi: 10.1038/s41586-024-07421-0.

Feng, Z., Zhou, H., Zhu, Z., Qian, J., and Mao, K. Unveiling and manipulating prompt influence in large language models. *arXiv preprint arXiv:2405.11891v1*, 2024.

Grattafiori, A., Dubey, A., Jauhri, A., Pandey, A., Kadian, A., Al-Dahle, A., Letman, A., Mathur, A., et al. The llama 3 herd of models. *arXiv preprint arXiv:2407.21783v3*, 2024.

Guo, C., Pleiss, G., Sun, Y., and Weinberger, K. Q. On calibration of modern neural networks. *arXiv preprint arXiv:1706.04599v2*, 2017.

Guo, J., Wu, Y., Qiu, J., Huang, K., Juan, X., Yang, L., and Wang, M. Temporal consistency for LLM reasoning process error identification. *arXiv preprint arXiv:2503.14495v1*, 2025.

Heo, J., Xiong, M., Heinze-Deml, C., and Narain, J. Do LLMs estimate uncertainty well in instruction-following? In *International Conference on Learning Representations*, 2024.

Hu, E. J., Shen, Y., Wallis, P., Allen-Zhu, Z., Li, Y., Wang, S., Wang, L., and Chen, W. LoRA: Low-rank adaptation of large language models. *arXiv preprint arXiv:2106.09685v2*, 2021.

Huang, J., Chen, X., Mishra, S., Zheng, H. S., Yu, A. W., Song, X., and Zhou, D. Large language models cannot self-correct reasoning yet. *arXiv preprint arXiv:2310.01798v2*, 2023.

Kadavath, S., Conerly, T., Askell, A., Henighan, T., Drain, D., Perez, E., Schiefer, N., Dodds, Z. H., DasSarma, N., Tran-Johnson, E., Johnston, S., El-Showk, S., Jones, A., Elhage, N., Hume, T., Chen, A., Bai, Y., Bowman, S., Fort, S., Ganguli, D., Hernandez, D., Jacobson, J., Kernion, J., Kravec, S., Lovitt, L., Ndousse, K., Olsson, C., Ringer, S., Amodei, D., Brown, T., Clark, J., Joseph,

N., Mann, B., McCandlish, S., Olah, C., and Kaplan, J. Language models (mostly) know what they know. *arXiv preprint arXiv:2207.05221v2*, 2022.

Khalifa, M., Agarwal, R., Logeswaran, L., Kim, J., Peng, H., Lee, M., Lee, H., and Wang, L. Process reward models that think. *arXiv preprint arXiv:2504.16828*, 2025.

Kossen, J., Han, J., Razzak, M., Schut, L., Malik, S., and Gal, Y. Semantic entropy probes: Robust and cheap hallucination detection in LLMs. *arXiv preprint arXiv:2406.15927v1*, 2024.

Kumar, A., Zhuang, V., Agarwal, R., Su, Y., Co-Reyes, J. D., Singh, A., Baumli, K., Iqbal, S., Bishop, C., Roelofs, R., Zhang, L. M., McKinney, K., Shrivastava, D., Paduraru, C., Tucker, G., Precup, D., Behbahani, F., and Faust, A. Training language models to self-correct via reinforcement learning. *arXiv preprint arXiv:2409.12917*, 2024.

Kumar, K. Detecting token-level hallucinations using variance signals: A reference-free approach. *arXiv preprint arXiv:2507.04137v3*, 2025.

Lester, B., Al-Rfou, R., and Constant, N. The power of scale for parameter-efficient prompt tuning. *arXiv preprint arXiv:2104.08691v2*, 2021.

Li, R., Long, J., Qi, M., Xia, H., Sha, L., Wang, P., and Sui, Z. Towards harmonized uncertainty estimation for large language models. In *Proceedings of the 63rd Annual Meeting of the Association for Computational Linguistics*, 2025a. doi: 10.18653/v1/2025.acl-long.1118. URL <https://aclanthology.org/2025.acl-long.1118/>.

Li, X. L. and Liang, P. Prefix-tuning: Optimizing continuous prompts for generation. *arXiv preprint arXiv:2101.00190v1*, 2021.

Li, Z., Shareghi, E., and Collier, N. Reasongraph: Visualisation of reasoning paths. *arXiv preprint arXiv:2503.03979v1*, 2025b.

Lightman, H., Kosaraju, V., Burda, Y., Edwards, H., Baker, B., Lee, T., Leike, J., Schulman, J., Sutskever, I., and Cobbe, K. Let's verify step by step. *arXiv preprint arXiv:2305.20050v1*, 2023.

Liu, D., Nassereldine, A., Yang, Z., Xu, C., Hu, Y., Li, J., Kumar, U., Lee, C., Chu, Z., Song, L., Xiao, C., Choi, Y., Chang, K.-W., Tsvetkov, Y., and Smith, N. A. Large language models have intrinsic self-correction ability. *arXiv preprint arXiv:2406.15673v2*, 2024a.

Liu, G., Qi, Z., Zhang, X., Cheng, L., and Johnson, K. M. Self-correction is not an innate capability in large language models. *arXiv preprint arXiv:2410.20513v7*, 2024b.

Ma, H., Liu, J., Fan, L., Wu, T.-H., Liang, F., and Wang, X. Semantic energy: Detecting LLM hallucination beyond entropy. *arXiv preprint arXiv:2508.14496*, 2025.

MacKay, D. J. C. *Information Theory, Inference, and Learning Algorithms*. Cambridge University Press, 2003. ISBN 9780521642989.

Malinin, A. and Gales, M. J. F. Predictive uncertainty estimation via prior networks. *arXiv preprint arXiv:1802.10501v2*, 2018.

Manakul, P., Liusie, A., and Gales, M. J. F. Selfcheck-gpt: Zero-resource black-box hallucination detection for generative large language models. *arXiv preprint arXiv:2303.08896v3*, 2023.

Mao, Z., Venkat, A., Bisliouk, A., Kothiyal, A., Subramanian, S. K., Singhu, S., and Ruchkin, I. Confidence over time: Confidence calibration with temporal logic for large language model reasoning, 2026.

Nikitin, A., Kossen, J., Gal, Y., and Marttinen, P. Kernel language entropy: Fine-grained uncertainty quantification for LLMs from semantic similarities. *arXiv preprint arXiv:2405.20003*, 2024.

Niu, M., Haddadi, H., and Pang, G. Robust hallucination detection in LLMs via adaptive token selection. *arXiv preprint arXiv:2504.07863*, 2025.

Olsson, C., Elhage, N., Nanda, N., Joseph, N., DasSarma, N., Henighan, T., Mann, B., Askell, A., Bai, Y., Chen, A., Conerly, T., Drain, D., Ganguli, D., Hatfield-Dodds, Z., Hernandez, D., Johnston, S., Jones, A., Kernion, J., Lovitt, L., Ndousse, K., Amodei, D., Brown, T., Clark, J., Kaplan, J., McCandlish, S., and Olah, C. In-context learning and induction heads. *arXiv preprint arXiv:2209.11895v1*, 2022.

Peng, J., Wang, M., Zhao, X., Zhang, K., Wang, W., Jia, P., Liu, Q., Guo, R., and Liu, Q. Stepwise reasoning error disruption attack of LLMs. *arXiv preprint arXiv:2412.11934v5*, 2024.

Quevedo, E., Yero, J., Quesada, A., and Martínez, Y. Detecting hallucinations in large language model generation: A token probability approach. *arXiv preprint arXiv:2405.19648*, 2024.

Shannon, C. E. A mathematical theory of communication. *The Bell System Technical Journal*, 27(3):379–423, 1948. doi: 10.1002/j.1538-7305.1948.tb01338.x.

Tyen, G., Mansoor, H., Cărbune, V., Chen, P., and Mak, T. LLMs cannot find reasoning errors, but can correct them given the error location. *arXiv preprint arXiv:2311.08516v3*, 2023.

Wang, X., Wei, J., Schuurmans, D., Le, Q., Chi, E., Narang, S., Chowdhery, A., and Zhou, D. Self-consistency improves chain of thought reasoning in language models. *arXiv preprint arXiv:2203.11171v4*, 2022.

Wei, J., Wang, X., Schuurmans, D., Bosma, M., Xia, F., Chi, E., Le, Q. V., and Zhou, D. Chain-of-thought prompting elicits reasoning in large language models. *arXiv preprint arXiv:2201.11903v6*, 2022.

Yang, A., Yang, B., Hui, B., Zheng, B., Yu, B., Zhou, C., Li, C., Li, C., Liu, D., Huang, F., Dong, G., Wei, H., Lin, H., Tang, J., Wang, J., Yang, J., Tu, J., Zhang, J., Ma, J., Yang, J., Xu, J., Zhou, J., Bai, J., He, J., Lin, J., Dang, K., Lu, K., Chen, K., Yang, K., Li, M., Xue, M., Ni, N., Zhang, P., Wang, P., Peng, R., Men, R., Gao, R., Lin, R., Wang, S., Bai, S., Tan, S., Zhu, T., Li, T., Liu, T., Ge, W., Deng, X., Zhou, X., Ren, X., Zhang, X., Wei, X., Ren, X., Liu, X., Fan, Y., Yao, Y., Zhang, Y., Wan, Y., Chu, Y., Liu, Y., Cui, Z., Zhang, Z., Guo, Z., and Fan, Z. Qwen2 technical report. *arXiv preprint arXiv:2407.10671v4*, 2024.

Yang, Z., Qi, P., Zhang, S., Bengio, Y., Cohen, W. W., Salakhutdinov, R., and Manning, C. D. Hotpotqa: A dataset for diverse, explainable multi-hop question answering. *arXiv preprint arXiv:1809.09600v1*, 2018.

Yao, S., Zhao, J., Yu, D., Du, N., Shafran, I., Narasimhan, K., and Wang, Y. React: Synergizing reasoning and acting in language models. *arXiv preprint arXiv:2210.03629v3*, 2022.

Yu, W., Jiang, Z., Dong, Y., and Feng, J. Reclor: A reading comprehension dataset requiring logical reasoning, 2020. URL <https://arxiv.org/abs/2002.04326>.

Zhang, Z., Zheng, C., Wu, Y., Zhang, B., Lin, R., Liu, B. Y. D., Zhou, J., and Lin, J. The lessons of developing process reward models in mathematical reasoning. *arXiv preprint arXiv:2501.07301*, 2025.

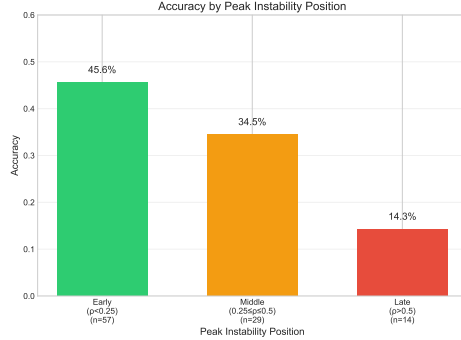


Figure 4. Accuracy by peak instability position on the 100-trace held-out baseline run (same setting as Table 2). Early peaks allow recovery and yield higher accuracy; late peaks leave insufficient time to recover.

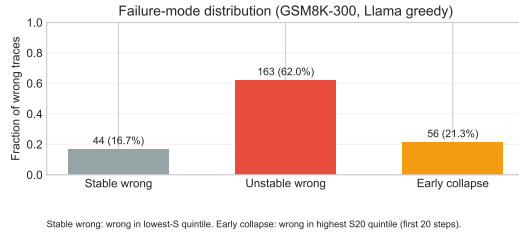


Figure 5. Failure-mode distribution on GSM8K (300 examples) for Llama-3.2-1B-Instruct greedy. We partition wrong traces into three disjoint categories for interpretability: *stable wrong* (wrong traces in the lowest quintile of instability strength S), *early collapse* (wrong traces in the highest quintile of early-window strength $S_{20} = \max_{t \leq 20} I_t$), and *unstable wrong* (the remaining wrong traces). This breakdown highlights that a non-trivial fraction of errors are stable wrong, consistent with the limitation that instability is not a universal explanation of failure.

A. Appendix: Additional Figures

Peak-timing visualization. Figure 4 visualizes the peak-timing effect reported in section 6: earlier peak positions are more recoverable and are associated with higher final-answer accuracy, while later peaks are associated with substantially lower accuracy, consistent with the “corrective vs. destructive” interpretation.

Failure-mode breakdown. Figure 5 provides a complementary view of error types in the same GSM8K-300 setting. It summarizes the stable-but-wrong, early-collapse, and dynamically unstable categories used in section A and discussed in section J.

B. Appendix: Theoretical Details

B.1. Theoretical Analysis: Dynamic Instability in Autoregressive Reasoning

We give a compact theoretical framing that connects internal trajectory instability to observable changes in next-token

distributions. The results below are intentionally limited in scope: they do not assert that instability causes failure, only that large observable distributional changes are consistent with substantial internal state changes, and that timing effects admit a simple recoverability interpretation. Proofs are provided in section C. These statements are not used to estimate hidden-state distances or to claim causal mechanisms. The goal is not to model Transformers in full detail, but to formalize two core ideas: observable shifts in next-token distributions are mathematically linked to changes in internal state under mild local conditions, and the timing of such shifts matters for recoverability under a finite decoding budget.

Where possible we state explicit constants, but our use of these results is qualitative: none of the bounds are used to set thresholds or guarantee prediction performance, and trajectory-dependent constants (e.g., curvature terms) may vary widely or degenerate in certain decoding regimes.

Autoregressive reasoning as a dynamical system. We model autoregressive inference as a discrete-time closed-loop system. Let $h_t \in \mathcal{H} \subseteq \mathbb{R}^d$ denote an unobserved internal state at generation step t and let x_t be the emitted token. The state evolves as

$$h_{t+1} = f(h_t, x_t). \quad (5)$$

The next-token distribution is obtained from logits z_t via an output map and softmax:

$$z_t = Wh_t + b, \quad p_t = \text{softmax}(z_t), \quad (6)$$

where $W \in \mathbb{R}^{V \times d}$ and V is the vocabulary size. In black-box settings we only observe \tilde{p}_t , a truncated and renormalized top- k approximation of p_t , and we therefore compute observables from \tilde{p}_t throughout.

Assumptions. We adopt the following local technical assumptions (standard in local stability analyses) only to make the bounds below well-defined.

- **(A1) Local smoothness.** The state transition $f(h, x)$ is locally differentiable with respect to h along the trajectories considered.
- **(A2) Observable gain of the output map.** Let $\Pi := I - \frac{1}{V} \mathbf{1} \mathbf{1}^\top$ be the projection onto $\mathbf{1}^\perp$ (removing the softmax shift invariance). There exists a local constant $\sigma_W > 0$ along the trajectories considered such that $\|\Pi W u\|_2 \geq \sigma_W \|u\|_2$ for all relevant state differences u .

These assumptions do not guarantee a global stability property for the model. They only support a local connection between changes in internal state and changes in observable

token distributions. We emphasize that (A2) is a strong, local identifiability-type condition: it may fail globally and need not hold uniformly over all directions u in practice, but is sufficient to formalize a stepwise link between hidden-state changes and projected logit changes.

Definitions: finite-horizon stability and local expansion.

Definition 1 (Finite-horizon stability). *Given a trajectory $(h_t)_{t=0}^T$, we say it is stable over horizon T if for any sufficiently small perturbation δh_0 there exists $C > 0$ such that*

$$\sup_{t \leq T} \|\delta h_t\|_2 \leq C \|\delta h_0\|_2. \quad (7)$$

Otherwise the trajectory is dynamically unstable over horizon T .

Definition 2 (Local expansion rate). *Let $J_f(h_t, x_t) := \frac{\partial f}{\partial h}(h_t, x_t)$ and define*

$$\alpha_t := \log \|J_f(h_t, x_t)\|_{\text{op}}. \quad (8)$$

When $\sum_{t=t_0}^{t_1} \alpha_t$ is large and positive, small perturbations expand rapidly over the interval, indicating an internally unstable segment.

These quantities are not directly observable in our black-box setting. We use them only to formalize what it means for an internal trajectory to be unstable.

From internal instability to observable distributional change.

Lemma 1 (Hidden-state change induces projected logit change). *Under (A2), for consecutive steps,*

$$\|z_t - z_{t-1}\|_{\perp} := \|\Pi(z_t - z_{t-1})\|_2 \geq \sigma_W \|h_t - h_{t-1}\|_2. \quad (9)$$

Lemma 2 (Observable distributional change reflects logit change). *Let $p_t = \text{softmax}(z_t)$ and $p_{t-1} = \text{softmax}(z_{t-1})$ be consecutive next-token distributions with logits $z_t, z_{t-1} \in \mathbb{R}^V$. Let Π denote the projection onto $\mathbf{1}^{\perp}$. Define the trajectory-dependent curvature constant*

$$\kappa_{t,\text{traj}} := \inf_{s \in [0, 1]} \lambda_{\min} \left(J(p(s)) \Big|_{\mathbf{1}^{\perp}} \right), \quad (10)$$

where $z(s) = z_{t-1} + s(z_t - z_{t-1})$, $p(s) = \text{softmax}(z(s))$, and $J(p) = \text{diag}(p) - pp^{\top}$ is the softmax Jacobian. This quantity captures the minimum local curvature of the softmax map along the segment between z_{t-1} and z_t . Then

$$\text{JSD}(p_t, p_{t-1}) \geq \frac{\kappa_{t,\text{traj}}^2}{8} \|z_t - z_{t-1}\|_{\perp}^2. \quad (11)$$

Remark. The constant $\kappa_{t,\text{traj}}$ is local and trajectory-dependent. When the next-token distribution is nearly deterministic (for example near termination), the softmax Jacobian becomes nearly singular on $\mathbf{1}^{\perp}$, so $\kappa_{t,\text{traj}}$ can approach

zero and the bound becomes loose. This is consistent with our goal of diagnosing large transitions during uncertain and decision-critical segments; we do not claim a uniform lower bound that holds across all decoding regimes.

Proposition 1 (Top- k analogue (restricted simplex)). *Let \tilde{p}_t and \tilde{p}_{t-1} be the renormalized top- k distributions supported on \mathcal{V}_t and \mathcal{V}_{t-1} . Let $\bar{\mathcal{V}} = \mathcal{V}_t \cup \mathcal{V}_{t-1}$ and view $\tilde{p}_t, \tilde{p}_{t-1}$ as distributions on $\bar{\mathcal{V}}$ by zero-padding outside each step's support. This embedding leaves each step's logged probabilities unchanged and provides a shared support for divergence computation. Since any distribution on the restricted simplex with strictly positive coordinates can be written as a softmax of finite logits (unique up to an additive constant), the statement of Lemma 2 applies verbatim on the restricted logit space $\mathbb{R}^{|\bar{\mathcal{V}}|}$, yielding*

$$\text{JSD}(\tilde{p}_t, \tilde{p}_{t-1}) \geq \frac{\tilde{\kappa}_{t,\text{traj}}^2}{8} \left\| \tilde{\Pi}_{\bar{\mathcal{V}}}(\tilde{z}_t - \tilde{z}_{t-1}) \right\|_2^2, \quad (12)$$

where $\tilde{\Pi}_{\bar{\mathcal{V}}}$ is the projection onto $\mathbf{1}^{\perp}$ in $\mathbb{R}^{|\bar{\mathcal{V}}|}$, \tilde{z}_t denotes logits restricted to $\bar{\mathcal{V}}$ up to an additive constant, and $\tilde{\kappa}_{t,\text{traj}}$ is defined from the softmax Jacobian on the restricted simplex.

We emphasize that the existence of such restricted logits is used only to justify the geometry of the mapping. The analysis does not require access to \tilde{z}_t in practice.

Theorem 1 (Observable instability lower-bounds internal step change). *Under (A2), for consecutive steps,*

$$\text{JSD}(p_t, p_{t-1}) \geq \frac{\kappa_{t,\text{traj}}^2 \sigma_W^2}{8} \|h_t - h_{t-1}\|_2^2. \quad (13)$$

This result formalizes why large consecutive-step distributional shifts are consistent with substantial internal state changes, supporting our use of $D_t = \text{JSD}(\tilde{p}_t, \tilde{p}_{t-1})$ as an observable proxy for regime shifts.

Entropy as a proxy for decision fragility.

Definition 3 (Decision margin). *Let $\Delta_t := z_{t,(1)} - z_{t,(2)}$ be the gap between the largest and second-largest logits at step t .*

Lemma 3 (Margin robustness). *If an additive logit perturbation η satisfies $\|\eta\|_{\infty} < \frac{1}{2}\Delta_t$, then the argmax token under greedy decoding does not change.*

Lemma 4 (Entropy upper-bounds peak confidence). *For any distribution P , $H(P) \geq -\log P_{\max}$, where $P_{\max} := \max_i P(i)$.*

High entropy therefore rules out a highly peaked distribution and is consistent with locally fragile decisions where several candidates are competitive. This motivates combining distributional change with an uncertainty term in $I_t = D_t + \lambda H_t$. Empirically, this complements D_t under top- k logging, consistent with our λ ablation.

Corrective vs. destructive instability and timing effects.

We interpret instability events as transitions between more stable basins of continuation. Let \mathcal{A}_G denote an empirical basin of internal states that tend to converge to correct answers and let \mathcal{A}_B denote an empirical basin of internal states that tend to converge to incorrect answers. A transition $\mathcal{A}_B \rightarrow \mathcal{A}_G$ corresponds to corrective instability, while a transition $\mathcal{A}_G \rightarrow \mathcal{A}_B$ corresponds to destructive instability.

Stabilization assumption. We formalize the recoverability intuition with a stylized stabilization-time assumption: entering (or re-entering) the good basin may require a minimum number of remaining steps before the trajectory reliably terminates correctly. Let **Correct** denote the event that the final answer at step T is correct. We assume there exist $\tau_{\text{mix}} \in \mathbb{N}$ and $\delta \in (0, 1)$ such that:

- **(S1) Sufficient budget implies high success.** For any step t , if $h_t \in \mathcal{A}_G$ and $T - t \geq \tau_{\text{mix}}$, then

$$\Pr(\text{Correct} \mid h_t \in \mathcal{A}_G, T - t \geq \tau_{\text{mix}}) \geq 1 - \delta. \quad (14)$$

- **(S2) Fresh entry with insufficient budget is unreliable.** There exists an entry subset $\mathcal{A}_G^{\text{entry}} \subseteq \mathcal{A}_G$ such that if $h_t \in \mathcal{A}_G^{\text{entry}}$ and $T - t < \tau_{\text{mix}}$, then

$$\Pr(\text{Correct} \mid h_t \in \mathcal{A}_G^{\text{entry}}, T - t < \tau_{\text{mix}}) \leq \delta. \quad (15)$$

Intuitively, τ_{mix} captures a finite-horizon stabilization or mixing time needed after a corrective transition before the trajectory reliably terminates correctly.

Theorem 2 (Late correction penalty). *Assume (S1) and (S2). If a corrective transition occurs at step t^* and $h_{t^*} \in \mathcal{A}_G^{\text{entry}}$ with $T - t^* < \tau_{\text{mix}}$, then the probability of producing a correct final answer is at most δ . Conversely, if $h_{t^*} \in \mathcal{A}_G$ and $T - t^* \geq \tau_{\text{mix}}$, then the success probability is at least $1 - \delta$.*

This formalizes the recoverability intuition underlying our empirical timing effect: late instability peaks are less recoverable given a limited remaining decoding budget.

Summary.

B.2. Implementation Note: Top- k Truncation

We use top- k logging because it is available in many black-box inference settings and keeps storage and compute tractable at per-step resolution. Truncation and renormalization can affect both entropy and JSD: when consecutive steps have low support overlap (high support-set turnover), computing divergences on the union of two renormalized top- k supports can amplify spikes relative to full vocabulary

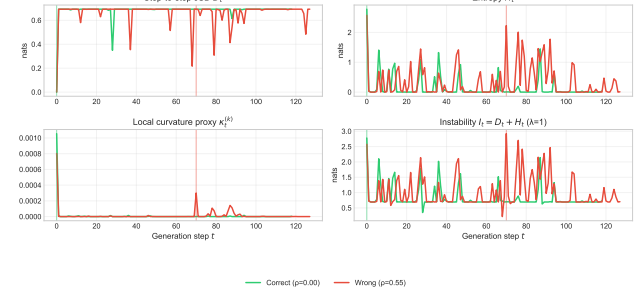


Figure 6. Theory and experiment alignment on representative Llama-3.2-1B-Instruct GSM8K greedy traces. We plot step-to-step JSD D_t , entropy H_t , the local softmax Jacobian curvature proxy $\kappa_t^{(k)}$ computed as the smallest non-zero eigenvalue of $\text{diag}(\tilde{p}_t) - \tilde{p}_t \tilde{p}_t^\top$ (equivalently, the minimum eigenvalue on $\mathbf{1}^\perp$) on the renormalized top- k distribution, and the combined instability $I_t = D_t + H_t$ (with $\lambda = 1$). The example traces are selected deterministically to illustrate an early-peak correct trace and a late-peak wrong trace. Large JSD spikes occur during uncertain segments where $\kappa_t^{(k)}$ is non-negligible, consistent with Lemma 2, and late peak position aligns with the recoverability interpretation in Theorem 2.

distributions. Intuitively, when the top candidates change substantially from one step to the next, the truncated distributions share little support, producing a large JSD spike.

To ensure our conclusions are not artifacts of a particular truncation choice, we run two validation checks. First, on held-out traces we validate the “corrective vs. destructive” timing effect using entropy/JSD computed from full vocabulary logits (no truncation; section 6). Second, we recompute the main signal from the same logged top-50 traces using smaller effective values of k (by truncating the logged list) and find qualitatively similar separability trends once k is moderately large (section E).

C. Appendix: Proofs

This appendix provides proofs for the theoretical statements in Appendix B.

C.1. Preliminaries: Softmax shift invariance

Softmax is invariant to adding constants: $\text{softmax}(z) = \text{softmax}(z + c\mathbf{1})$ for any scalar c . We therefore measure logit differences on the identifiable subspace $\mathbf{1}^\perp := \{v \in \mathbb{R}^V : \langle v, \mathbf{1} \rangle = 0\}$ using the projection

$$\Pi := I - \frac{1}{V}\mathbf{1}\mathbf{1}^\top, \quad \|u\|_\perp := \|\Pi u\|_2. \quad (16)$$

C.2. Proof of projected logit lower bound on Jensen–Shannon divergence

Proof of Lemma 2. Fix consecutive logits z and z' with $p = \text{softmax}(z)$ and $q = \text{softmax}(z')$. Define the line

Table 3. How the theoretical statements relate to the main empirical findings.

Empirical observation	Theoretical intuition
JSD spikes predict failure trends	Theorem 1
High entropy indicates fragile decisions	Lemmas above on margin and entropy
Not all instability is harmful	Basin interpretation and timing
Late peaks are associated with lower accuracy	Theorem 2

segment $z(s) = z' + s(z - z')$ for $s \in [0, 1]$ and let $p(s) = \text{softmax}(z(s))$. Define

$$\kappa_{t,\text{traj}} := \inf_{s \in [0, 1]} \lambda_{\min}(J(p(s))|_{\mathbf{1}^\perp}), \quad (17)$$

where $J(p) = \text{diag}(p) - pp^\top$ is the softmax Jacobian. By definition, for any $v \in \mathbf{1}^\perp$ and any $s \in [0, 1]$ we have $v^\top J(p(s))v \geq \kappa_{t,\text{traj}} \|v\|_2^2$. Let $m = \frac{1}{2}(p + q)$. By definition,

$$\text{JSD}(p, q) = \frac{1}{2}\text{KL}(p\|m) + \frac{1}{2}\text{KL}(q\|m). \quad (18)$$

Pinsker's inequality (constants differ by convention) gives $\text{KL}(p\|m) \geq 2\text{TV}(p, m)^2$ and $\text{KL}(q\|m) \geq 2\text{TV}(q, m)^2$, where $\text{TV}(a, b) = \frac{1}{2}\|a - b\|_1$ (and we use natural logarithms). Any equivalent Pinsker constant convention would lead to the same qualitative conclusion up to universal factors. Since $p - m = \frac{1}{2}(p - q)$ and $q - m = \frac{1}{2}(q - p)$, we have

$$\text{JSD}(p, q) \geq \frac{1}{2}\text{TV}(p, q)^2 = \frac{1}{8}\|p - q\|_1^2 \geq \frac{1}{8}\|p - q\|_2^2. \quad (19)$$

It remains to lower-bound $\|p - q\|_2$ by $\|z - z'\|_\perp$. Consider the path $z(s) = z' + s(z - z')$ for $s \in [0, 1]$ and define $p(s) = \text{softmax}(z(s))$. Then

$$\begin{aligned} p - q &= p(1) - p(0) \\ &= \int_0^1 \frac{d}{ds} p(s) ds \\ &= \int_0^1 J(p(s))(z - z') ds, \end{aligned} \quad (20)$$

where $J(p) = \nabla_z \text{softmax}(z) = \text{diag}(p) - pp^\top$ is the softmax Jacobian. Because $J(p)\mathbf{1} = 0$, only the projected component matters: $J(p(s))(z - z') = J(p(s))\Pi(z - z')$. Let $v := \Pi(z - z') \in \mathbf{1}^\perp$. Then

$$p - q = \int_0^1 J(p(s))v ds. \quad (21)$$

Taking the inner product with v and using symmetry of $J(p(s))$ yields

$$\begin{aligned} \langle p - q, v \rangle &= \int_0^1 v^\top J(p(s))v ds \\ &\geq \int_0^1 \kappa_{t,\text{traj}} \|v\|_2^2 ds \\ &= \kappa_{t,\text{traj}} \|v\|_2^2, \end{aligned} \quad (22)$$

Since $J(p(s))\mathbf{1} = 0$, we interpret $\lambda_{\min}(J(p(s))|_{\mathbf{1}^\perp})$ as the smallest eigenvalue over unit vectors orthogonal to $\mathbf{1}$. By Cauchy-Schwarz, $\|p - q\|_2\|v\|_2 \geq \langle p - q, v \rangle$, hence

$$\|p - q\|_2 \geq \kappa_{t,\text{traj}}\|v\|_2 = \kappa_{t,\text{traj}}\|z - z'\|_\perp. \quad (23)$$

Combining the two bounds gives

$$\text{JSD}(p, q) \geq \frac{1}{8}\|p - q\|_2^2 \geq \frac{\kappa_{t,\text{traj}}^2}{8}\|z - z'\|_\perp^2, \quad (24)$$

as claimed. \square

C.3. Proof of the late correction penalty

Let Correct denote the event that the final answer is correct at step T .

Proof of Theorem 2. Let t^* be the step at which a corrective transition occurs, so that $h_{t^*} \in \mathcal{A}_G^{\text{entry}}$. Assume $T - t^* < \tau_{\text{mix}}$. By (S2), for any realization of $h_{t^*} \in \mathcal{A}_G^{\text{entry}}$, let E denote the event $T - t^* < \tau_{\text{mix}}$. Then

$$\Pr(\text{Correct} \mid h_{t^*}, E) \leq \delta. \quad (25)$$

Taking expectation over the randomness of h_{t^*} and applying the law of total probability,

$$\begin{aligned} \Pr(\text{Correct} \mid E) &= \mathbb{E}_{h_{t^*}} [\Pr(\text{Correct} \mid h_{t^*}, E)] \\ &\leq \delta. \end{aligned} \quad (26)$$

This proves the late correction penalty. Conversely, if $h_{t^*} \in \mathcal{A}_G$ and $T - t^* \geq \tau_{\text{mix}}$, then (S1) yields

$$\Pr(\text{Correct} \mid h_{t^*} \in \mathcal{A}_G, T - t^* \geq \tau_{\text{mix}}) \geq 1 - \delta. \quad (27)$$

\square

D. Appendix: Detector Comparison

The derivative-based change-point detector produces frequent detections, while CUSUM is much more conservative under the current thresholds. In our experiments, the binary change-point label is less predictive than continuous strength, reinforcing the decision to focus on strength-based analyses in the main text.

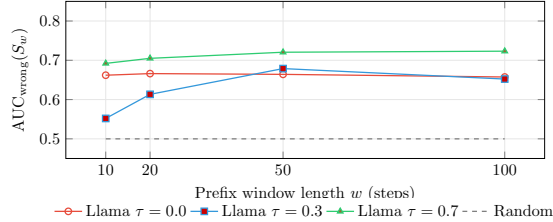


Figure 7. Early-warning separability as a function of prefix window length on GSM8K-300. We report $AUC_{\text{wrong}}(S_w)$ as a function of the window size w . Separability emerges with short prefixes and improves with longer windows, supporting that instability is detectable before completion of the full reasoning trace.

E. Appendix: Top- k Sensitivity

To validate truncation effects, we recompute the instability strength $S = \max_t I_t$ from the same logged top-50 traces using smaller effective values of k by truncating the stored list. Table 4 shows that the diagnostic signal weakens for very small k but is qualitatively stable once k is moderately large.

Top- k sensitivity across models. As an additional check, we recompute the diagnostic from full-set GSM8K baseline runs while varying the diagnostic truncation level k . Table 5 shows that AUC_{wrong} and rank association change only slightly between $k \in \{20, 50, 100\}$ across all evaluated models, supporting that our conclusions are not artifacts of a particular top- k choice.

F. Appendix: Early-Window Separability

To further control for length confounds, we compute $S_{50} = \max_{t \leq 50} I_t$, the max instability within the first 50 steps, and evaluate separability using the same AUC_{wrong} metric as in table 1. The signal remains predictive under this early-window restriction (table 6).

G. Appendix: Negative Controls and Alternative Baselines

This appendix reports two reviewer-oriented controls on GSM8K (300 examples) using the same logged traces as the main results for Llama-3.2-1B-Instruct greedy. First, we include time-structure negative controls by randomizing the temporal order and recomputing strength statistics. Second, we compare against simple entropy-family baselines computed from the same per-step observables without rerunning the models.

G.1. Time-Structure Negative Controls

Because the peak-based strength statistic $S = \max_t I_t$ is invariant to permutations of the sequence values, time-

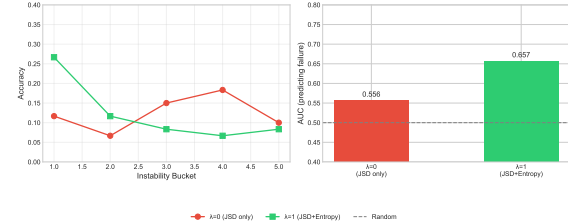


Figure 8. Signal ablation on Llama-3.2-1B-Instruct: comparing JSD-only ($\lambda = 0$) vs. JSD+Entropy ($\lambda = 1$). The entropy component improves discrimination, particularly in lower-instability buckets where pure JSD may saturate.

structure controls are most informative for timing-aware or windowed statistics (e.g., S_w and peak position ρ), rather than for S itself. We consider two temporal randomizations. (1) **Shuffle** $\{p_t\}$: for each trace we randomly permute the per-step logged top- k distributions before recomputing H_t , D_t , and I_t . (2) **Shuffle** $\{I_t\}$: for each trace we compute the original I_t sequence and then randomly permute it. Since the main strength statistic $S = \max_t I_t$ is invariant to permutations of I_t , this control primarily targets windowed statistics such as S_{50} . All shuffles are deterministic per example identifier.

G.2. Entropy-Family Baselines

We compare our main strength statistic $S_I = \max_t I_t$ against three simple alternatives computed from the same traces: $S_H = \max_t H_t$ (max entropy), $S_{\Delta H} = \max_t |H_t - H_{t-1}|$ (max entropy change), and $S_D = \max_t D_t$ (max JSD). We also report the early-window variants obtained by restricting the max to the first 50 steps. We report both full-trace and fixed early-window variants below.

G.3. Signal Ablation (Additional)

H. Appendix: Bootstrap Confidence Intervals

To quantify uncertainty under the GSM8K 300-example setting, we compute percentile bootstrap confidence intervals over examples (1000 resamples) for AUC_{wrong} and bucketed accuracy. Table 11 reports AUC confidence intervals for S and S_{50} , and Figure 9 visualizes bucket accuracy with 95% confidence intervals.

I. Appendix: Peak Threshold Sensitivity

We evaluate the robustness of the peak-timing interpretation by sweeping early and late thresholds for the peak position $\rho = t^*/T$ on the 100-trace full-vocabulary baseline run used in Table 2. Table 12 shows that early-peak traces consistently achieve higher accuracy than late-peak traces across a small threshold grid. We also plot accuracy as a function of peak position in 10 equal-width bins (figure 10).

Table 4. Top- k sensitivity on Llama-3.2-1B-Instruct greedy (GSM8K, 300 traces). Larger k yields a more stable estimate of entropy/JSD and slightly stronger separability; the overall trend remains.

Effective k	AUC _{wrong}	Spearman
10	0.626	-0.144
20	0.635	-0.154
50	0.657	-0.178

Table 5. Diagnostic top- k sensitivity across models on GSM8K (full test set, $N=1319$). We recompute $S = \max_t I_t$ using different diagnostic truncation levels k and report separability. All quantities are computed from the logged top- k distributions at inference time. Within each model block, shaded cells indicate the best value across diagnostic k for that metric (higher AUC; more negative Spearman).

Model	diag k	Acc	AUC _{wrong} (S)	Spearman(S)
Llama-3.2-1B-Inst	20	0.419	0.653	-0.262
	50	0.419	0.662	-0.277
	100	0.419	0.665	-0.283
Llama-3.2-3B-Inst	20	0.707	0.691	-0.300
	50	0.707	0.698	-0.312
	100	0.707	0.700	-0.315
Llama-3.1-8B-Inst	20	0.749	0.684	-0.276
	50	0.749	0.689	-0.284
	100	0.749	0.691	-0.286
Qwen2.5-0.5B-Inst	20	0.301	0.717	-0.344
	50	0.301	0.716	-0.343
	100	0.301	0.715	-0.341
Qwen2.5-1.5B-Inst	20	0.416	0.639	-0.237
	50	0.416	0.641	-0.241
	100	0.416	0.642	-0.242
Qwen2.5-7B-Inst	20	0.500	0.642	-0.245
	50	0.500	0.644	-0.249
	100	0.500	0.644	-0.249

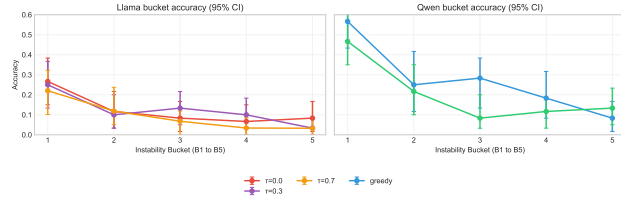


Figure 9. Bootstrap confidence intervals for bucketed accuracy on GSM8K (300 examples). Each curve plots accuracy across five equal-sized instability buckets (B1 to B5), with 95% bootstrap confidence intervals over examples (1000 resamples).

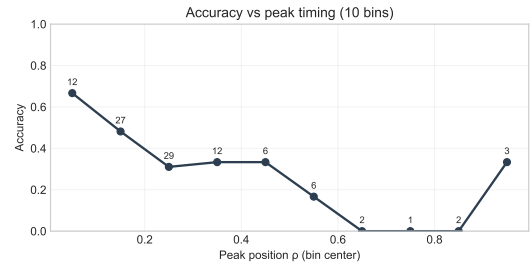


Figure 10. Accuracy by peak position $\rho = t^*/T$ in 10 equal-width bins on the 100-trace full-vocabulary baseline run. Bin counts are annotated above each point.

J. Appendix: Mechanistic Interpretation

The discussion in the main text provides a brief, non-committal mechanistic interpretation of the signal. Here we provide a longer interpretation, emphasizing that these abstractions do not imply a unique internal mechanism.

Closed-loop amplification. Autoregressive decoding is a feedback system: the emitted token becomes part of the next input, updating the residual stream and attention con-

text, and therefore the next-token distribution. In this view, regime shifts correspond to discrete reconfigurations of the effective computation performed by attention and MLP blocks, which can amplify local sensitivity in the state update map.

Decision fragility and near ties. Our instability signal combines realized distributional change with uncertainty. When top candidates are close in score, small state changes

Table 6. Early-window separability using $S_{50} = \max_{t \leq 50} I_t$ (GSM8K, 300 traces). AUC remains above chance under the fixed early-window restriction.

Model	Decoding	$\text{AUC}_{\text{wrong}}(S)$	$\text{AUC}_{\text{wrong}}(S_{50})$
Qwen2.5-1.5B-Inst	greedy	0.681	0.605
Llama-3.2-1B-Inst	$\tau = 0.0$	0.657	0.665

Table 7. Time-structure negative controls on GSM8K (300 examples) for greedy decoding. Bucket slope is measured as the accuracy difference between bucket B5 and B1. Shuffling $\{I_t\}$ does not affect $S = \max_t I_t$ by definition.

Model	Setting	$\text{AUC}_{\text{wrong}}(S)$	Spearman	B5–B1
Llama-3.2-1B-Instruct	original	0.657	-0.178	-0.183
Llama-3.2-1B-Instruct	shuffle $\{p_t\}$	0.652	-0.173	-0.150
Llama-3.2-1B-Instruct	shuffle $\{I_t\}$	0.657	-0.178	-0.183

can flip the argmax. In a Transformer, such near ties can arise when multiple partial solutions remain compatible with the prefix, leading to competing attention patterns and feature activations. In this regime, entropy is a proxy for proximity to a decision boundary, and it complements JSD when divergence estimates are compressed under top- k logging.

Route switching and local curvature. Large distributional shifts can reflect route switching, where attention reallocates from one subset of context tokens to another as the model commits to an intermediate value or revises an earlier step. Prior work suggests that Transformers can implement discrete, circuit-like behaviors in context (Olsson et al., 2022), which is compatible with abrupt changes in the effective computation and observed JSD spikes.

Basins and stabilization time. The basin sets \mathcal{A}_G and \mathcal{A}_B and the stabilization time τ_{mix} provide a compact way to state the recoverability intuition behind corrective versus destructive instability. In a Transformer, these basins can be interpreted as regions of residual-stream activation space that reliably produce continuations consistent with a correct or incorrect solution. The stabilization time can be interpreted as the number of subsequent steps required for the model to propagate a corrected intermediate value through the remaining reasoning and final-answer formatting, which explains why late instability peaks are less recoverable.

K. Appendix: Peak-Step Probes

To probe differences at the peak step $t^* = \arg \max_t I_t$, we analyze two additional metrics: margin drops and support-set turnover.

(Log-)probability margin drop. Let $\Delta_t = \log \tilde{p}_t^{(1)} - \log \tilde{p}_t^{(2)}$ be the gap between the top-2 log probabilities at

step t under the renormalized top- k distribution \tilde{p}_t . Here $\tilde{p}_t^{(1)}$ and $\tilde{p}_t^{(2)}$ denote the largest and second-largest probabilities under \tilde{p}_t (ranked values), not powers. We measure the *margin drop* $\Delta_{t^*-1} - \Delta_{t^*}$ as a proxy for how abruptly the model transitions from a locally dominant next-token preference to a more competitive state. We use log probabilities under \tilde{p}_t as a black-box proxy; analyzing raw logit margins would require white-box access but is conceptually aligned with the same mechanistic interpretation.

Support-set turnover. Let \mathcal{T}_t be the top-10 token set at step t . We compute the Jaccard *overlap* $J = |\mathcal{T}_{t^*} \cap \mathcal{T}_{t^*-1}| / |\mathcal{T}_{t^*} \cup \mathcal{T}_{t^*-1}|$, and define turnover as $1 - J$. We use top-10 here to focus on the most competitive candidates at the peak step, while \tilde{p}_t in our main signal uses top- k (typically $k = 50$) for a more stable entropy/JSD estimate. High turnover implies low consecutive-step support overlap, which contributes directly to large JSD spikes under truncated distributions.

Table 13 reveals a key distinction: **correct traces exhibit larger margin drops** (1.82 vs. 1.05) at the peak step t^* , while **wrong traces exhibit higher support-set turnover** (84% vs. 82%). We treat these metrics as descriptive characterizations; some effect sizes (e.g., turnover) are modest, but the patterns are consistent under pooling across decoding settings.

L. Appendix: Additional Full-Set Runs

To complement the main analyses, we report dense per-step baseline runs for six models on the full GSM8K test set (1319 examples) and on the HotpotQA distractor validation split (7405 examples). For each example we compute $S = \max_t I_t$ from the logged per-step instability and evaluate separability via $\text{AUC}_{\text{wrong}}$. We also report $S_{50} = \max_{t \leq 50} I_t$ as an early-window control, and bucket accuracy by five equal-sized quantile buckets of S . Hot-

Table 8. Time-structure negative controls on GSM8K (300 examples) for greedy decoding, evaluated with the early-window statistic $S_{50} = \max_{t \leq 50} I_t$. Shuffling reduces early-window separability, consistent with the role of temporal organization in windowed diagnostics.

Model	Setting	AUC _{wrong} (S_{50})	Spearman (S_{50})	B5–B1 (S_{50})
Llama-3.2-1B-Instruct	original	0.664	-0.187	-0.167
Llama-3.2-1B-Instruct	shuffle $\{p_t\}$	0.641	-0.161	-0.133
Llama-3.2-1B-Instruct	shuffle $\{I_t\}$	0.617	-0.134	-0.117

Table 9. Entropy-family baselines on GSM8K (300 examples) for greedy decoding. JSD-only statistics are near chance, consistent with our λ ablation.

Model	Statistic	AUC _{wrong} (S)	Spearman(S)
Llama-3.2-1B-Instruct	$S_I = \max_t I_t$	0.657	-0.178
Llama-3.2-1B-Instruct	$S_H = \max_t H_t$	0.650	-0.171
Llama-3.2-1B-Instruct	$S_{\Delta H} = \max_t H_t - H_{t-1} $	0.563	-0.072
Llama-3.2-1B-Instruct	$S_D = \max_t D_t$	0.511	-0.015

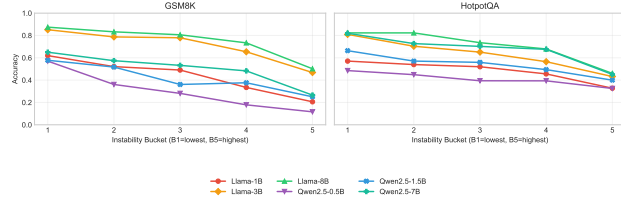


Figure 11. Bucketed accuracy trends for the full-set runs in Table 14. Each curve plots accuracy across five equal-sized instability buckets (B1 to B5), showing a monotonic decline as instability increases on both tasks and for all models.

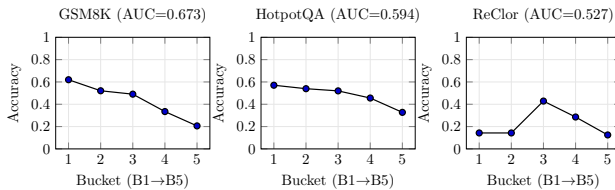


Figure 12. Cross-task validation on a fixed model (Llama-3.2-1B). We plot bucketed accuracy trends (B1 to B5) by instability strength on GSM8K, HotpotQA, and ReClor. On GSM8K and HotpotQA, accuracy declines with instability. On ReClor in this short-answer multiple-choice setting, the trend inverts: most errors are stable-but-wrong, and the rare correct traces exhibit higher instability.

potQA correctness uses a short-answer match on the first line of the generated output after normalization, with a containment check against the reference. The results of these full-set runs are summarized below.

M. Appendix: Peak Position in a Fixed Early Window

To control for time-budget confounds in the “corrective vs. destructive” analysis, we compute peak position within a fixed early window (first 50 steps). Let $t_{50}^* =$

$\arg \max_{t \leq 50} I_t$ (breaking ties by the smallest t) and $\rho_{50} = t_{50}^*/50$ on the same held-out baseline run as Table 2. The qualitative ordering remains: later peak positions *within the same window* correspond to lower accuracy (table 15).

N. Appendix: Reproducibility and Implementation Details

All results are generated via the project scripts in this repository with fixed configuration files for dataset, model, decoding settings, and logging parameters. The pipeline consists of: (i) generating traces by logging per-step top- k token log probabilities during decoding, (ii) computing H_t , D_t , and I_t from the renormalized top- k distributions as described in the Method section, and (iii) aggregating per-trace statistics (S and early-window variants), bucket summaries, and figures used in the paper. Unless otherwise noted, we use the GSM8K test split with 300 problems, log top-50 tokens per-step, and cap generation at 128 new tokens. The full-set runs use the GSM8K test split (1319 examples) and the HotpotQA distractor validation split (7405 examples), evaluated with the same per-trace metrics and bucket procedure. For stochastic decoding we use temperature $\tau = 0.7$ with nucleus sampling ($p = 0.9$) and a fixed random seed; for Llama-3.2-1B-Instruct we additionally run $\tau = 0.3$ under the same p and seed. We also include a small full vocabulary validation run for key timing claims (section 6).

Table 10. Entropy-family baselines on GSM8K (300 examples) for greedy decoding, evaluated in the fixed early window (first 50 steps).

Model	Statistic	$AUC_{\text{wrong}}(S_{50})$	Spearman(S_{50})
Llama-3.2-1B-Instruct	$S_{50,I} = \max_{t \leq 50} I_t$	0.664	-0.187
Llama-3.2-1B-Instruct	$S_{50,H} = \max_{t \leq 50} H_t$	0.648	-0.169
Llama-3.2-1B-Instruct	$S_{50,\Delta H} = \max_{t \leq 50} H_t - H_{t-1} $	0.544	-0.050
Llama-3.2-1B-Instruct	$S_{50,D} = \max_{t \leq 50} D_t$	0.418	0.140

 Table 11. Bootstrap confidence intervals for AUC_{wrong} on GSM8K (300 examples). Intervals are percentile 95% confidence intervals over 1000 bootstrap resamples.

Model	Decoding	AUC_{wrong}	
		(S)	(S_{50})
Llama-3.2-1B-Instruct	$\tau = 0.0$	0.657 [0.553, 0.756]	0.664 [0.545, 0.769]
Llama-3.2-1B-Instruct	$\tau = 0.3$	0.667 [0.571, 0.757]	0.679 [0.584, 0.772]
Llama-3.2-1B-Instruct	$\tau = 0.7$	0.741 [0.636, 0.834]	0.721 [0.614, 0.808]

 Table 12. Peak-timing threshold sweep on the 100-trace full-vocabulary baseline run. Gap denotes $Acc_{\text{early}} - Acc_{\text{late}}$.

Early ρ	Late ρ	N_{early}	Acc_{early}	N_{late}	Acc_{late}	Gap
0.20	0.45	39	0.538	19	0.211	0.328
	0.50	39	0.538	14	0.143	0.396
	0.60	39	0.538	8	0.125	0.413
0.25	0.45	57	0.456	19	0.211	0.246
	0.50	57	0.456	14	0.143	0.313
	0.60	57	0.456	8	0.125	0.331
0.30	0.45	68	0.441	19	0.211	0.231
	0.50	68	0.441	14	0.143	0.298
	0.60	68	0.441	8	0.125	0.316

 Table 13. Peak-step characteristics for correct vs. wrong traces (Llama-3.2-1B-Instruct, GSM8K). We aggregate 300 problems across three decoding settings (greedy; and stochastic sampling with $\tau \in \{0.3, 0.7\}$, top- p 0.9), yielding 900 traces. Correct traces show larger margin drops (decisive transition); wrong traces show higher turnover (chaotic support-set change). (For per-setting robustness across this grid, see Table 1; here we pool settings for mechanistic characterization.)

	Margin at t^*	Margin drop	Jaccard overlap	Turnover ($1 - J$)
Correct	0.30	1.82	0.18	0.82
Wrong	0.45	1.05	0.16	0.84

 Table 14. Dense per-step runs on GSM8K and HotpotQA (full test/validation splits), plus a ReClor validation subset (300 examples) for Llama-3.2-1B-Instruct under stochastic decoding. We report separability via AUC_{wrong} for the full-trace peak strength $S = \max_t I_t$ and an early-window control $S_{50} = \max_{t \leq 50} I_t$.

Model	Dataset	N	AUC_{wrong}		Spearman	AUC_{wrong} (S_{50})
			Accuracy	(S)		
Llama-3.2-1B-Inst	GSM8K	1319	0.434	0.673	-0.298	0.615
Llama-3.2-3B-Inst	GSM8K	1319	0.707	0.687	-0.295	0.618
Llama-3.1-8B-Inst	GSM8K	1319	0.749	0.692	-0.288	0.598
Qwen2.5-0.5B-Inst	GSM8K	1319	0.301	0.714	-0.341	0.654
Qwen2.5-1.5B-Inst	GSM8K	1319	0.416	0.643	-0.244	0.565
Qwen2.5-7B-Inst	GSM8K	1319	0.500	0.644	-0.250	0.581
Llama-3.2-1B-Inst	HotpotQA	7405	0.483	0.594	-0.163	0.594
Llama-3.2-3B-Inst	HotpotQA	7405	0.632	0.662	-0.271	0.662
Llama-3.1-8B-Inst	HotpotQA	7405	0.704	0.675	-0.277	0.675
Qwen2.5-0.5B-Inst	HotpotQA	7405	0.410	0.568	-0.116	0.575
Qwen2.5-1.5B-Inst	HotpotQA	7405	0.537	0.603	-0.179	0.603
Qwen2.5-7B-Inst	HotpotQA	7405	0.675	0.654	-0.250	0.654
Llama-3.2-1B-Inst	ReClor	300	0.027	0.054	0.250	0.046

Table 15. Accuracy by peak position within a fixed early window (same 100-trace full vocabulary baseline as Table 2). Even when peak position is defined within the first 50 steps, later peaks are associated with lower accuracy.

Peak Position (first 50 steps)	% of Traces	Accuracy
Early ($\rho_{50} < 0.25$)	13%	0.54
Middle ($0.25 \leq \rho_{50} \leq 0.5$)	34%	0.47
Late ($\rho_{50} > 0.5$)	53%	0.28